gebiology

Geobiology (2016), **14**, 276–292 DOI: 10.1111/gbi.12171

# Limited influence of Si on the preservation of Fe mineral-encrusted microbial cells during experimental diagenesis

A. PICARD,* M. OBST, G. SCHMID, F. ZEITVOGEL AND A. KAPPLER

*Center for Applied Geoscience, Eberhard Karls University Tübingen, Tübingen, Germany*

## ABSTRACT

The reconstruction of the history of microbial life since its emergence on early Earth is impaired by the difficulty to prove the biogenicity of putative microfossils in the rock record. While most of the oldest rocks on Earth have been exposed to different grades of diagenetic alterations, little is known about how the remains of micro-organisms evolve when exposed to pressure (P) and temperature (T) conditions typical of diagenesis. Using spectroscopy and microscopy, we compared morphological, mineralogical, and chemical biosignatures exhibited by Fe mineral-encrusted cells of the bacterium *Acidovorax* sp. BoFeN1 after long-term incubation under ambient conditions and after experimental diagenesis. We also evaluated the effects of Si on the preservation of microbial cells during the whole process. At ambient conditions, Si affected the morphology but not the identity (goethite) of Fe minerals that formed around cells. Fe-encrusted cells were morphologically well preserved after 1 week at 250 °C-140 MPa and after 16 weeks at 170 °C-120 MPa in the presence or in the absence of Si. Some goethite transformed to hematite and magnetite at 250 °C-140 MPa, but in the presence of Si more goethite was preserved. Proteins—the most abundant cellular components—were preserved over several months at ambient conditions but disappeared after incubations at high temperature and pressure conditions, both in the presence and in the absence of Si. Other organic compounds, such as lipids and extracellular polysaccharides seemed well preserved after exposure to diagenetic conditions. This study provides insights about the composition and potential preservation of microfossils that could have formed in Fe- and Si-rich Precambrian oceans.

Received 22 May 2015; accepted 10 November 2015

Corresponding author: A. Picard. Tel.: +1 (617) 495 9266; fax: +1 (617) 495 8848; e-mail: apicard@fas.harvard.edu

*Present address: Department of Organismic and Evolutionary Biology, Harvard University, 16 Divinity Avenue, Cambridge, MA 02138, USA

## INTRODUCTION

Reports of extremely well-preserved ancient micro-organisms and even potentially new shapes of microbial life in siliceous rock layers of the 1.9-Ga-old Gunflint formation have triggered tremendous interest in understanding the process of cell preservation by Si (Barghoorn & Tyler, 1965; Brasier *et al.*, 2015). Microbial silicification has been studied in natural environments, such as hot springs (Phoenix *et al.*, 2003; Konhauser *et al.*, 2004) and deep-sea sediments (Westall *et al.*, 1995) or mimicked in laboratory experiments (Oehler & Schopf, 1971; Francis *et al.*, 1978; Westall *et al.*, 1995; Orange *et al.*, 2009, 2013a,b). When micro-organisms are incubated in solutions containing various concentrations of Si, encrustation starts with the precipitation of silica colloids onto the cell surface, followed by the formation of silica gel by polymerization. Eventually cellular components become completely impregnated by crystalline Si compounds (Konhauser & Jones, 2011). For a good preservation of the morphology, silicification of cells must occur quickly; however, once silicified, cells can be preserved for several years (Orange *et al.*, 2014). Although cells are recognizable after encrustation, only the cell wall is well preserved, and internal features seem to disappear (Konhauser & Jones, 2011; Orange *et al.*, 2014). Various groups in the Bacteria and Archaea domains have been fossilized in silica, such as Cyanobacteria, Aquificae, Firmicutes, or Euryarchaeota (e.g., Francis *et al.*, 1978; Westall *et al.*, 1995; Toporski *et al.*, 2002; Lalonde *et al.*, 2005; Orange *et al.*, 2009) and it is generally accepted that

micro-organisms play a passive role in silicification (Konhauser & Jones, 2011). However, as cell surface composition varies among micro-organisms, the initial precipitation of Si colloids might vary as well, leading to different degrees of silicification depending on the type of micro-organism considered (Konhauser *et al.*, 2004; Konhauser & Jones, 2011 and references therein).

In natural environments, silicified micro-organisms are also found associated with Fe minerals (Ferris *et al.*, 1986; Fortin *et al.*, 1998; Konhauser, 1998). The most common phases associated with micro-organisms in sediments, river biofilms, hot springs, or hydrothermal deposits are Fe, Al silicates of varying crystallinities (e.g., Ferris *et al.*, 1987; Konhauser & Ferris, 1996; Fortin *et al.*, 1998; Konhauser *et al.*, 1998). It is suggested that the formation of these phases around cells starts with the primary fixation of cations, such as $Fe^{3+}$, on the functional groups of the outer membrane or cell wall, followed by the secondary fixation of silicate groups onto the cations that serve as nucleation sites (Urrutia & Beveridge, 1993, 1994; Fein *et al.*, 2002). The fixation of cations to anionic groups at the surface of the cells seems to inhibit the activity of catalytic enzymes and appears to be essential for the preservation of Archaea and Bacteria in silica (Ferris *et al.*, 1988; Orange *et al.*, 2011). This is highly relevant for the preservation of microbial remains in the past, as Precambrian oceans before 1.8 Ga contained high concentrations of both Fe and Si (Holland, 1973; Siever, 1992; Maliva *et al.*, 2005).

The hunt for microfossils in the rock record has been pursued for several decades to reconstruct the different steps in the evolution of life and metabolisms (Westall, 2008). Given the small size of micro-organisms and the limited morphological diversity in the microbial world, the biogenicity of microbial-like structures is difficult to establish. An excellent example for this challenge is illustrated by cell-like structures in the famous 3.46-Ga Apex chert proposed to be microfossils, based on the analysis of thick sections (Schopf, 1993; Schopf *et al.*, 2002). Recent nanoscale structural and chemical analyses of these putative microfossils using transmission electron microscopy (TEM) rather suggest that these structures are indistinguishable from vermiform phyllosilicate grains grown during hydrothermal alteration of the deposit (Brasier *et al.*, 2002, 2015). There is, however, still debate regarding the carbon associated with these mineral structures (Brasier *et al.*, 2015). Although microbial fossilization studies show a general good preservation of micro-organisms at ambient conditions, and even for long periods of time (Orange *et al.*, 2014), preservation in the rock record also requires a limited degradation of microbial remains under diagenetic conditions. Very few studies have addressed that question (Oehler & Schopf, 1971; Oehler, 1976; Beveridge *et al.*, 1983; Li *et al.*, 2013, 2014; Picard *et al.*, 2015). Although there is no means to reproduce the effects of geological times in the laboratory, experimental diagenesis experiments, performed at high temperature (T) and pressure (P), provide useful information about the evolution of microbial shape and composition and about what can be expected in the rock record. In this study, we evaluated the preservation potential of bacteria encrusted in Fe minerals under T–P conditions simulating sediment burial and rock formation. For that purpose, we used the bacterium *Acidovorax* sp. BoFeN1 which forms Fe(III)-mineral crusts around cells when exposed to Fe(II) during growth (Kappler *et al.*, 2005). The early steps of Fe biomineralization have been well characterized at high resolution (Miot *et al.*, 2011; Pantke *et al.*, 2012; Klueglein *et al.*, 2014; Schmid *et al.*, 2014). The evolution of organic compounds in Fe mineral-encrusted BoFeN1 cells after short heating experiments has been recently reported (Li *et al.*, 2013). Additionally we assessed whether the presence of Si during the formation of the Fe crust had an impact on the preservation of Fe-encrusted cells for several months at ambient conditions and for 1–16 weeks under experimental diagenetic conditions. Scanning electron microscopy (SEM), confocal laser scanning microscopy (CLSM), Raman spectroscopy, and scanning transmission X-ray microscopy (STXM) aimed to determine mineralogical and chemical changes occurring in bacteria as a function of temperature and pressure.

## MATERIALS AND METHODS

### Microbial strain and cultivation

Strain *Acidovorax* sp. BoFeN1, a nitrate-reducing Fe(II)-oxidizing bacterium isolated from freshwater lake sediments (Kappler *et al.*, 2005), came from our laboratory culture collection. Strain BoFeN1 was grown in anoxic freshwater mineral medium, as described by Ehrenreich and Widdel (Ehrenreich & Widdel, 1994). Instead of 0.5 g $L^{-1}$, $KH_2PO_4$ was decreased to 0.14 g $L^{-1}$, and NaCl was added at 0.2 g $L^{-1}$ to maintain the ionic strength (Hohmann *et al.*, 2010). Fe(II) was added to the medium at an initial concentration of 10 mM from a sterile stock solution of $FeCl_2$. After formation of white precipitates, identified as vivianite (Miot *et al.*, 2009), the medium was filtered in an anoxic glove box and distributed in 25-mL aliquots into 58-mL serum bottles. Acetate and nitrate were added to serum bottles from sterile stock solutions at a final concentration of 5 and 10 mM, respectively. Amorphous Si was added to the medium at a final concentration of 2 mM from a suspension of $Na_2SiO_3 \cdot 9H_2O$ prepared at pH 7.0. A preculture, transferred and grown twice at 30 °C in medium without Fe, was used to inoculate bottles of medium containing Fe and Fe+Si. Cultures were incubated at 30 °C and atmospheric pressure. These cultures were sampled after 1, 9, and 19 months for SEM, after 12 and 17 months for Raman spectroscopy, after 19 months for

STXM, and after 21 months for CLSM. Aliquots of the same cultures were taken after 2, 6, 7, and 21 months to perform diagenesis experiments at 130 °C-100 MPa (1 week), 170 °C-120 MPa (16 weeks), 250 °C-140 MPa (1 week), and 170 °C-120 MPa (4 weeks), respectively.

### Loading of bacterial cultures in gold capsules

Gold capsules (~3 cm long) were cut from gold tubes (inner diameter 2.1 mm, outer diameter 2.5 mm; Wieland Edelmetalle GmbH, Pforzheim, Germany) previously combusted at 800 °C for 4 h to remove organic residues used for processing. Capsules were sealed at one extremity by tungsten inert gas welding, sonicated in ethanol, and dried at 60 °C prior to filling. Bacterial cultures were left to settle before sampling, so organo-mineral precipitates could be concentrated at the bottom of the bottle. Cultures were neither centrifuged nor washed. Approximately ~100 μL of concentrated culture, withdrawn from the culture bottle with sterile needles and syringes, was immediately transferred into the capsule. The second extremity of the capsules was quickly clamped to remove gas space and transported to the welding apparatus. The whole procedure was performed under ambient atmosphere. The cell density in the capsules could not be determined as some loss occurred during the welding process of the second extremity.

#### *Experimental diagenesis and preparation of samples for analytical measurements*

Experimental diagenesis was performed in a hydrothermal autoclave (SITEC 01603-1500-R300 °C; SITEC-Sieber Engineering AG, Ebmatingen, Switzerland) that comprised three independent reactors. Gold capsules containing samples were placed into the reactors of the autoclave. Pressure was increased after the reactors reached the target temperature (usually after 1–2 h). Independent incubations were performed for 1 week at up to 250 °C and 140 MPa. Long incubations of 4 and 16 weeks were performed at 170 °C-120 MPa. After incubation, capsules were opened with a razor blade cleaned with ethanol and samples were recovered using sterile micropipettes. Samples were (i) air-dried on glass slides for Raman spectroscopy, (ii) rinsed with sterile deionized water, and air-dried on glass coverslips that were subsequently mounted on aluminum stubs with conductive double-side carbon tape for SEM, (iii) rinsed with sterile deionized water and air-dried on 200-mesh Cu TEM grids with a support film in pure Formvar (Plano, Wetzlar, Germany) for STXM, and (iv) stained in their original wet state by fluorescent dyes for CLSM.

#### *Scanning electron microscopy*

Samples were sputter-coated with ~8 nm of Pt with a BalTec SCD 005 sputter coater (BalTec, Balzers, Liechtenstein) and imaged with a LEO 1450 VP scanning electron microscope equipped with a tungsten hairpin filament (now Zeiss, Oberkochen, Germany) at the Department of Geosciences of the University of Tübingen. Secondary electron images were obtained at an acceleration voltage of 5 kV with a working distance of 3–4 mm using an Everhart–Thornley secondary electron detector. Imaging was performed on samples deposited on coverslips mounted on stubs, as described above, and samples on TEM grids (after STXM measurements were performed at the synchrotron) mounted on a custom-made scanning transmission electron microscopy (STEM) sample holder for SEM. Although the imaging procedure is similar for both sample supports, the background of images differs. SEM images of cells prepared on glass slides attached to carbon tape have a dark background, while SEM images of cells imaged on TEM grids have a bright background.

### Raman spectroscopy

Raman spectroscopy is a well-established method for the characterization of Fe minerals (Das & Hendry, 2011). The mineralogy of the samples was characterized on an Alpha300 Raman spectrometer (WITec, Ulm, Germany) at the Department of Pharmaceutical Technology (University of Tübingen). The excitation source was a 534-nm-line laser with power of light evaluated at <1 mW on the sample. The spectrometer was equipped with charged coupled device (CCD) and 1800 grooves $mm^{-1}$ grating. Each Raman spectrum was an average of two acquisitions of 60 s. Goethite (86–88%, Bayferrox 920 Z), magnetite (98%, Bayferrox E8710; LANXESS Inorganic Pigments, Krefeld, Germany), and hematite (Fluka > 99%) were used as reference compounds and measured as dry powders on a glass slide.

#### *Confocal laser scanning microscopy*

Z-stacks of images were acquired on a Leica SPE confocal laser scanning microscope (CLSM; Leica Microsystems, Wetzlar, Germany) equipped with 405, 488, 561, and 635 nm lasers and a 63× water immersion lens with a numerical aperture of 1.15 at the Center for Applied Geoscience (Environmental and Analytical Microscopy group, University of Tübingen). The fluorescent probes NanoOrange® stain, wheat germ agglutinin Alexa Fluor® 633 conjugates (WGA-633), and FM®4-64 stain, used to detect proteins, polysaccharides, and lipids, respectively, were purchased from Molecular Probes®, Life Technologies™.

#### *Scanning transmission X-ray microscopy and near-edge X-ray absorption fine structure spectroscopy*

Scanning transmission X-ray microscopy and near-edge X-ray absorption fine structure (NEXAFS) spectroscopy were done at the STXM 5.3.2.2 beamline of the Advanced Light Source (Berkeley, CA, USA). Details on the

beamline are given elsewhere (Kilcoyne *et al.*, 2003). Image sequences (stacks) were recorded on cells across the C K-edge (280–320 eV) and the O K-edge (530–560 eV), with a spectral resolution of 0.1 eV in regions of interest, to gain information on the distribution of cellular components and minerals, respectively. To map the distribution of Fe, images were recorded both below the Fe $L_{3,2}$ edges, at 704 eV, and at the main absorption peak of Fe(III) oxyhydroxides at the $L_2$ edge at 723.8 eV. Additionally, reference spectra at the O K-edge were acquired at the STXM beamline of the Canadian Light Source (CLS; Kaznatcheev *et al.*, 2007).

### Data analysis

Scanning transmission X-ray microscopy and NEXAFS data were processed using the aXis2000 software package (Hitchcock, 2015). Images were converted from transmission scale to linear absorbance scale [optical density (OD)], using the equation: $OD = -\ln(I/I_0)$, where OD is the optical density of an individual pixel, $I$ is the intensity of the transmitted photons, and $I_0$ is the intensity measured in an empty area adjacent to the sample. Average NEXAFS spectra were extracted from whole image sequences collected across the C K-edge and the O K-edge and fitted to a linear combination of standard spectra. For that purpose, we used the 'singular value decomposition' or singular value decomposition (SVD) function in aXis2000. The standard spectra of xanthan (used as polysaccharide standard), albumin (used as protein standard), 1,2-dipalmotoyl-sn-glycero-3-phosphocholine (used as lipid standard), and aragonite (used as carbonate standard), provided by others (Lawrence *et al.*, 2003; Dynes *et al.*, 2006; Obst *et al.*, 2009), gave the best results for data analysis at the C K-edge. Reference spectra of synthetic Fe minerals—hematite, goethite, and magnetite—provided the best results for fitting analyses at the O K-edge. After determining which standard spectra provide the best fitting results, quantitative maps were derived from images sequences using the SVD function in aXis2000, as described in other studies (Lawrence *et al.*, 2003; Dynes *et al.*, 2006).

To determine whether the size of cells changed as function of experimental conditions, the length of individual cells was measured on SEM images. A total of 30–352 cells were measured for each experimental condition, depending on the number of SEM images available. A one-way analysis of variance (ANOVA) was performed with the Kaleidagraph application ($F = 3.4030223$, $P = 0.0004$). The Dunnett post hoc test was chosen to determine whether the mean of one group (BoFeN1 cells grown in Fe—ambient conditions), designated as the control group, differs significantly from each of the means of the other groups. If the $P$-value of the test is lower than 0.05, there is thus a significant difference between the groups. Data are summarized in Table S1.

## RESULTS

### Preservation of cell morphology during aging at ambient conditions and during experimental diagenesis

The bacterium *Acidovorax* sp. BoFeN1 was cultivated with Fe(II) in the absence or presence of Si (hereafter called Fe and Fe+Si cultures, respectively). Over the course of several months, the morphology of cells was evaluated using SEM. Mineral crusts that formed around cells did not significantly change over the course of 19 months (Fig. 1). Spike-shaped crusts were typically observed in the Fe cultures (Fig. 1A,C,E), while round mineral aggregates formed around the cells in the Fe+Si cultures (Fig. 1B,D, F). The same cultures were subsampled several times and the culture aliquots were used to perform diagenesis experiments at temperatures (T) and pressures (P) of up to 250 °C and 140 MPa, respectively, and for up to 16 weeks. After experimental diagenesis, the general morphology of bacterial cells from Fe cultures and from Fe+Si cultures was preserved after 1 week at the highest T–P conditions of 250 °C and 140 MPa (Fig. 2G,H) as well as after 4-week and 16-week long incubations at 170 °C and 120 MPa (Fig. 2C–F). A few cells from the Fe culture incubated at 170 °C-120 MPa for 4 and 16 weeks appeared cracked open (Fig. 2C,E). The difference in morphology observed between Fe- and Fe+Si-grown cultures at ambient conditions was preserved after experimental diagenesis. The evolution of the cell length was analyzed as a function of T–P conditions (Fig. 3, Table S1). The cells were significantly longer only in the Fe+Si culture after 16-week incubation at 170 °C-120 MPa.

### Evolution of mineralogy with increasing T–P conditions

In both cultures, with and without Si, orange precipitates formed within a few days after inoculation, but did not change color afterward at ambient conditions. Minerals in the Fe culture attached to the bottom of the glass serum bottles, while minerals in the Fe+Si culture did not (see Fig. S1 showing bottles after shaking). This suggested a difference in charge of mineral aggregates and/or a difference in mineral aggregate structure between Fe and Fe+Si precipitates, which leads to a different affinity to the glass wall. Raman spectra of 12-month and 17-month cultures showed the spectral features of goethite in both Fe and Fe+Si cultures as a result of Fe(II) oxidation by BoFeN1 (Fig. 4 displays spectra acquired after 12 months at ambient conditions). The Raman spectrum of ferrihydrite has one broad feature that is at a different wavenumber than any peak from other reference spectra. Although it is not possible to completely rule out the presence of ferrihydrite after 12–17 months at ambient conditions, we can affirm that ferrihydrite is not present at levels detectable by

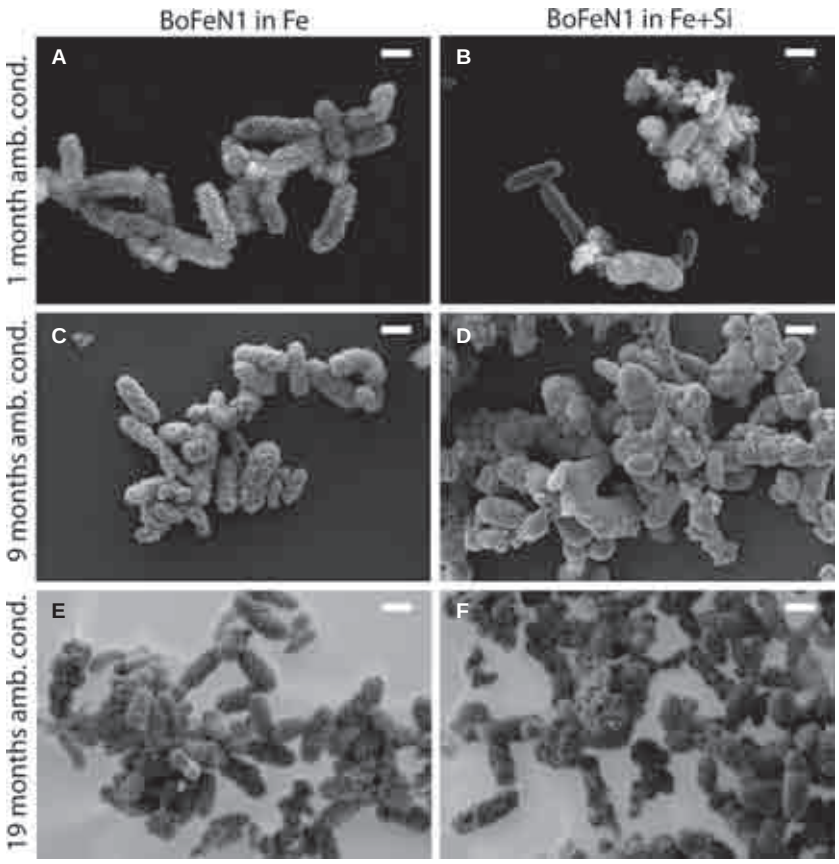


**Fig. 1** SEM images of BoFeN1 cells grown in Fe (A, C, E) and Fe+Si (B, D, F). Cells appear well preserved after 1 month (A, B), 9 months (C, D), and 19 months (E, F) at ambient conditions. Si affects the morphology of the mineral crust around cells. Images E and F were acquired from samples deposited on formvar-coated TEM grids for STXM measurements and therefore have a lighter background than images A–D that were acquired from samples deposited on glass slides attached to a stub. Scale bar = 1 μm on all images. SEM, scanning electron microscopy; TEM, transmission electron microscopy; STXM, scanning transmission X-ray microscopy.

Raman spectroscopy. In samples incubated under diagenetic conditions, goethite was the only mineral detectable up to 170 °C-120 MPa, including in the sample incubated for 16 weeks, while it transformed to hematite and magnetite after 1 week at 250 °C-140 MPa. Some goethite appeared to be preserved as shown by the Raman signal (Fig. 4).

To investigate the mineralogy at the cellular level, NEXAFS spectra, extracted from image sequences recorded at the O K-edge, were analyzed (Fig. 5). At ambient conditions, the best match for the sample spectrum was the goethite spectrum, although peaks are not as intense as those of the reference spectrum. The ferrihydrite spectrum did not match the sample spectrum and resulted in higher residual signals when used for the fitting procedure. The spectra of the samples incubated at the highest T–P conditions were fitted to a linear combination of goethite, hematite, and magnetite spectra. While hematite (~76%) dominated the Fe culture after the highest T–P treatment, goethite (~51%) was still the major component preserved in the Fe+Si culture after the T–P treatment (Table 1). The proportion of magnetite in the T–P-treated Fe+Si culture (31%) was twice as the T–P-treated Fe culture (15%). Component maps derived from the fitting analysis of image sequences recorded across the O K-edge revealed variable distributions of each Fe mineral (Fig. 6). While hematite seemed to be mainly present close to the cells, the remaining goethite appears to be around cells, perhaps in the extracellular polymeric substances (EPS) remains surrounding cells (see last paragraph in the result section). Magnetite appears to be distributed homogeneously close to and around cells (Fig. 6). Altogether, these results suggest that Fe(III) reduction had occurred during experimental diagenesis, probably coupled to the oxidation of organic matter. The variable localization of minerals is possibly a result of local differences in organic carbon concentration and variable thicknesses of Fe minerals.

### Distribution of organic and inorganic carbon as a function of T–P conditions

To investigate the evolution of the carbon chemistry in cells, the NEXAFS spectra at the C K-edge of whole cells were extracted from image sequences (Fig. 7). At ambient conditions, the main absorption peaks at 285.2 and 288.2 eV, assigned to $1s \rightarrow \pi^*$ excitations of C=C in aromatic groups and $1s \rightarrow \pi^*$ excitations of C=O adjacent to peptide bonds, respectively, were indicative of the presence of proteins, both in the absence and presence of Si. A third peak was observed at 290.4 eV and was indicative of the

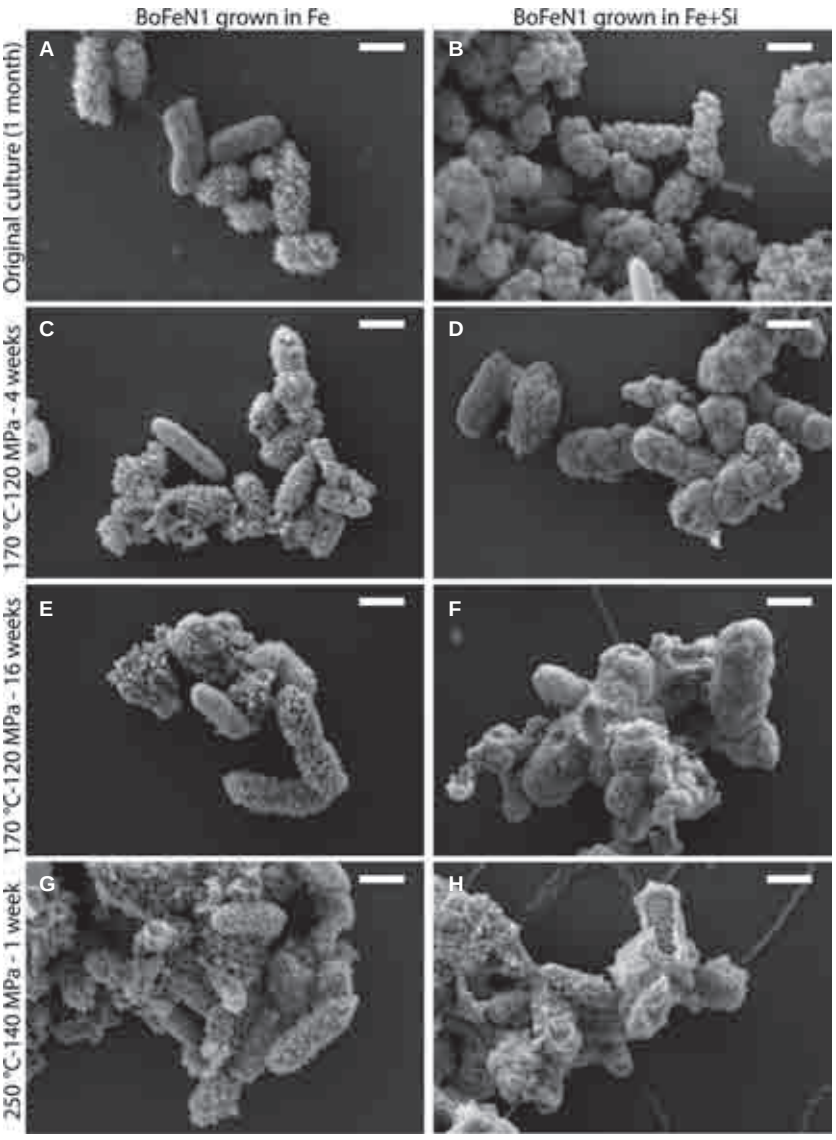


**Fig. 2** Scanning electron microscopy (SEM) images of BoFeN1 cells before and after experimental diagenesis. Cells grown in Fe (A) and Fe+Si (B) were submitted to 170 °C-120 MPa for 4 weeks (C, D) and for 16 weeks (E, F) and to 250 °C-140 MPa for 1 week (G, H). SEM images in panels A and B are from the same samples as panels A and B of Fig. 1, respectively. Cells appear well preserved at all conditions. The difference in morphology of the mineral crust around cells caused by Si is preserved after incubations at high T–P conditions. Scale bar = 1 μm on all images.

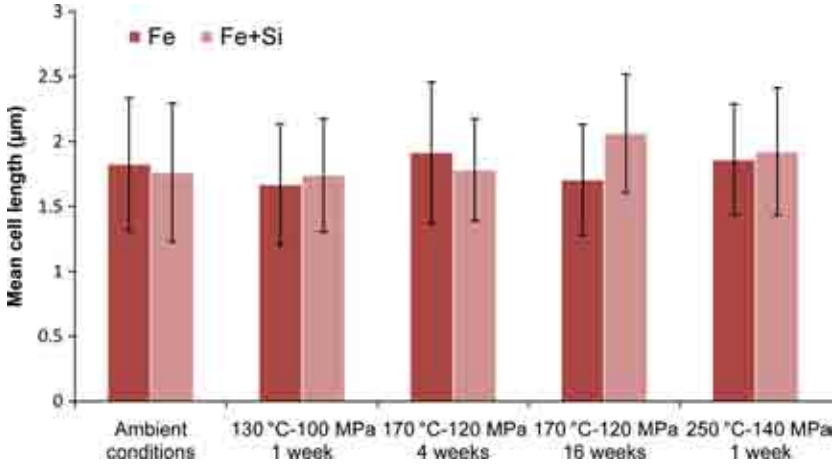


**Fig. 3** Average cell length (μm) as a function of temperature and pressure conditions. An ANOVA performed with a Dunnett test revealed that only cells grown in Fe+Si and incubated for 16 weeks at 170 °C-120 MPa increased in size in comparison with the ambient conditions. See Table S1 for data.

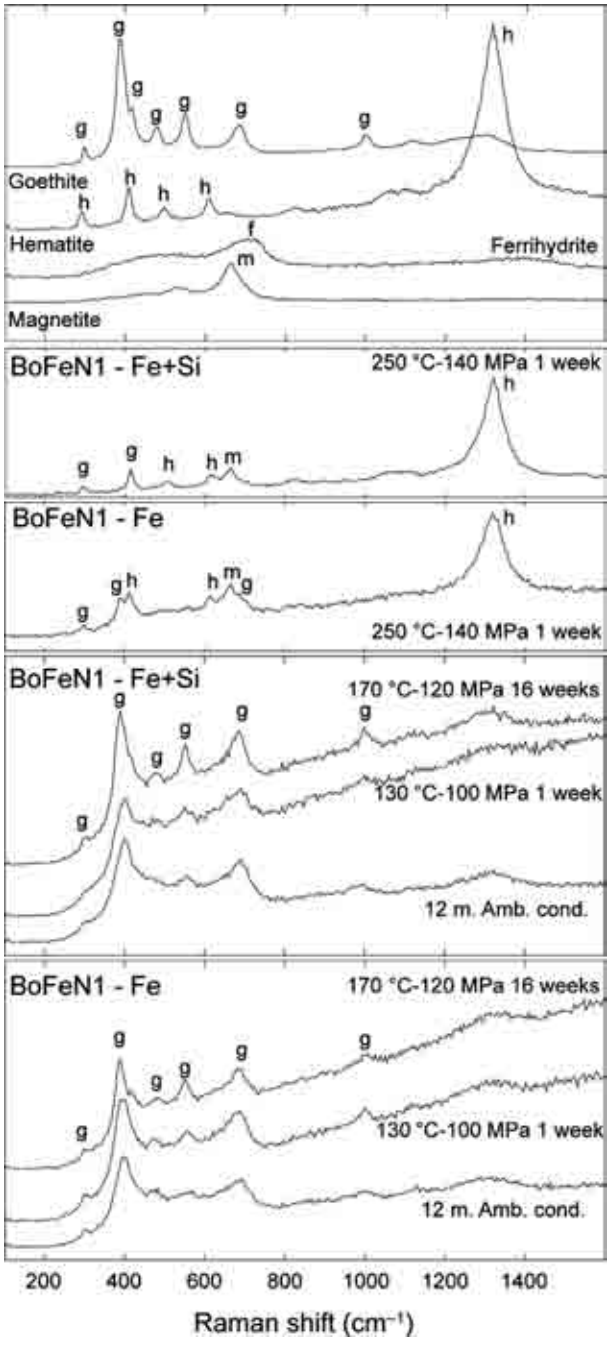


**Fig. 4** Raman spectra of dried BoFeN1 cultures grown in Fe and in Fe+Si, after 12 months at ambient conditions, and after incubations at high T–P conditions. Raman spectra of hematite, goethite, ferrihydrite, and magnetite were acquired on synthetic powders. Transformation of goethite to hematite occurs above 170 °C-120 MPa. Goethite is still present after 1 week at 250 °C-140 MPa.

1s→π* excitation of C=O in carbonates. Additional less intense spectral features occurred at 288.6 eV and at 287.4 eV and were interpreted as carboxylic and aliphatic C, assigned to polysaccharide and most likely saturated lipids, respectively (Lehmann *et al.*, 2009). Linear combi-

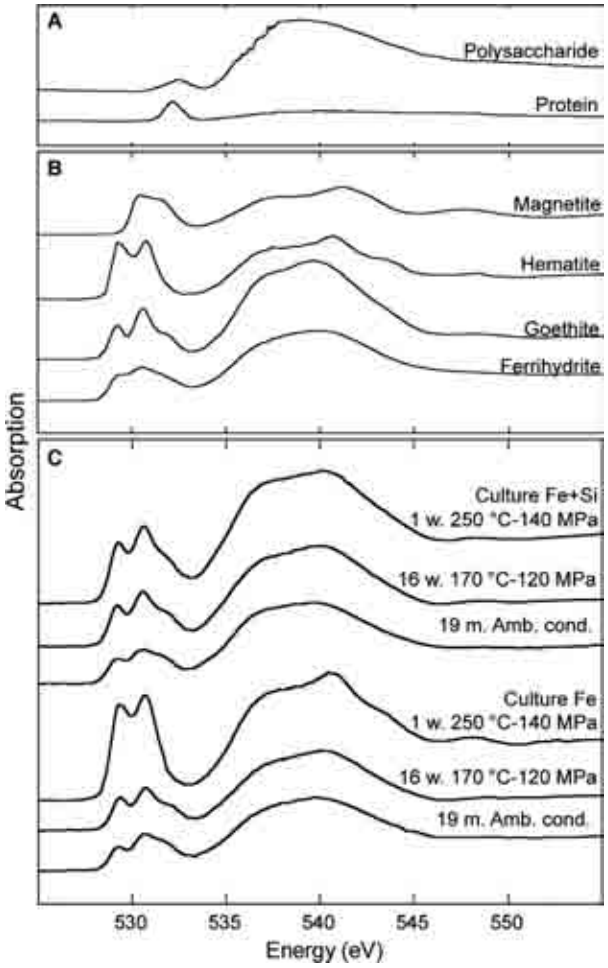


**Fig. 5** NEXAFS spectra at the O K-edge. (A) Reference spectra for protein (albumin) and polysaccharide (xanthan). (B) Reference spectra for ferrihydrite, goethite, hematite, and magnetite. (C) Spectra of BoFeN1 cells grown in Fe and Fe+Si before and after incubations under diagenetic conditions. The original cultures kept at ambient conditions were 19 months old at the time of measurement. Spectra recorded after 1 week at 250 °C-140 MPa show a significant difference in mineralogy between cells originally grown in Fe and in Fe+Si. NEXAFS, near-edge X-ray absorption fine structure.

**Table 1** Results of the LCF analyses performed on NEXAFS spectra at the O K-edge extracted from image sequences acquired on samples incubated for 1 week at 250 °C and 140 MPa. Normalized standard spectra of goethite, hematite, and magnetite were used. Results are given as calculated percentages

| Experimental conditions | Goethite (%) | Hematite (%) | Magnetite (%) |
|---|---|---|---|
| Culture grown in Fe | | | |
| 250 °C-140 MPa 1 week | 9 | 76 | 15 |
| Culture grown in Fe+Si | | | |
| 250 °C-140 MPa 1 week | 51 | 18 | 31 |

NEXAFS, near-edge X-ray absorption fine structure; LCF, linear combination fitting.

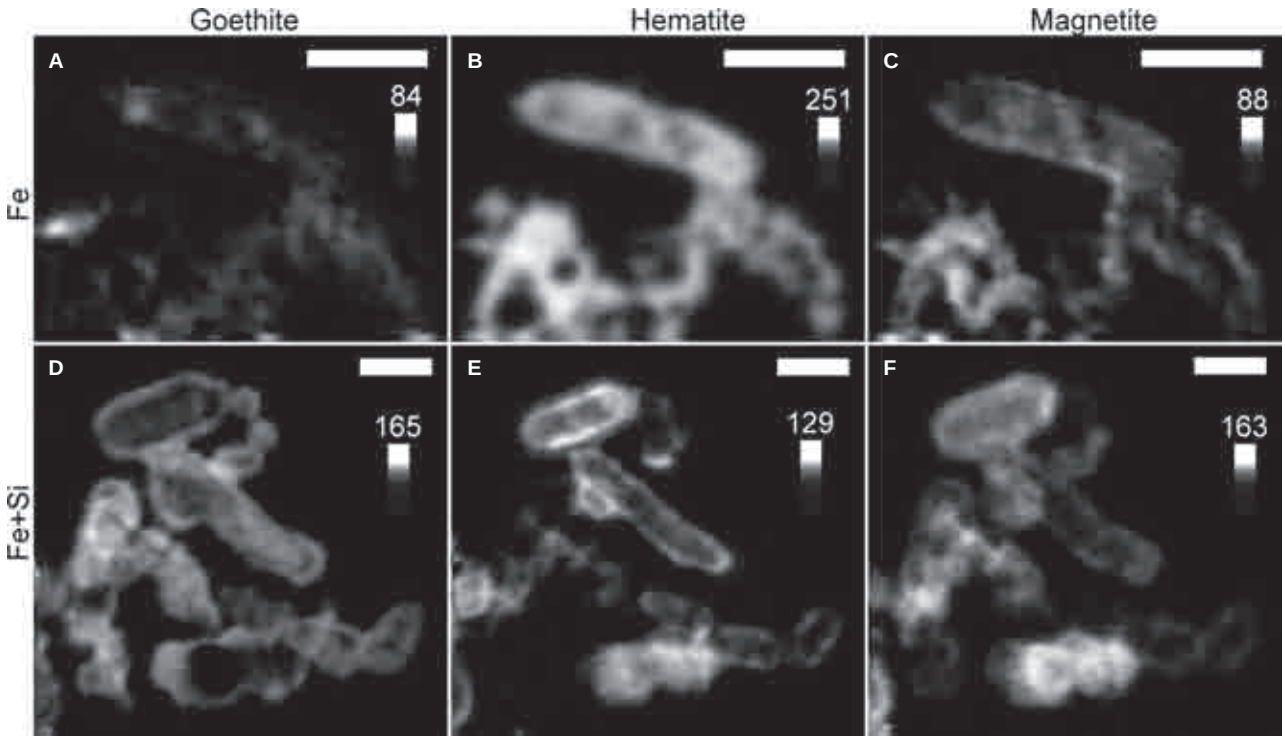


**Fig. 6** Component maps of goethite, hematite, and magnetite in cells of the Fe and Fe+Si cultures incubated for 1 week at 250°C-140 MPa, as derived by LCF of image sequences measured across the O K-edge (525–555 eV). The scales indicate thickness in nm. Scale bars = 1 μm on all images. LCF, linear combination fitting.

nation fitting (LCF) analysis of the NEXAFS spectra at the C K-edge showed a larger proportion of the protein and polysaccharide components and a lower proportion of the lipid component in the culture grown in Fe than in the culture grown in Fe+Si (Table 2). It also revealed a small contribution of a carbonate standard spectrum to the NEXAFS spectra of BoFeN1 cells grown in Fe and Fe+Si. Component maps showed that proteins were mainly associated with cells, while polysaccharides and lipids were present at the periphery of cells and in extracellular aggregates, in association with Fe (Figs 8 and 9). Carbonate was also associated with the Fe-mineral phase (Figs 8 and 9). As a complementary approach, we used CLSM to map the distribution of cellular components, such as proteins, polysaccharides, and lipids, using appropriate fluorescent dyes. No difference between cells grown in Fe and cells grown in Fe+Si at ambient conditions was observed (Fig. 10). Polysaccharides seem to be very abundant on cells, as shown by the dominance of the red fluorescent signal in samples at ambient conditions in the RGB overlay (Fig. 10).

Based on NEXAFS spectra at the C K-edge, we observed significant changes in the organic composition of the cells with increasing T–P conditions. The 'protein peak' at 288.2 eV, typically present at ambient conditions, disappeared after incubations under T–P conditions, while the 'polysaccharide peak' at 288.6 eV and the 'lipid shoulder' at 287.4 eV became clearly apparent (Fig. 7). The proportion of the remaining components, lipid, polysaccharide, and carbonate was similar in samples originating both from the Fe and Fe+Si cultures (Table 2). The remaining organic components polysaccharide and lipid appeared to be distributed homogenously in cells (Figs S2 and S3). Fe appeared more abundant on cells that looked heavily encrusted in the SEM images (Figs S2 and S3). Carbonate appeared colocalized with Fe after 16 weeks at 170 °C-120 MPa, while it seemed homogenously distributed after 1 week at 250 °C-140 MPa. In the CLSM images, the decreasing fluorescence signal of the protein dye indicated that the protein content decreased with increasing T–P conditions (Fig. 10), similar to the STXM data. The decrease in fluorescence intensity seemed to be more important with increasing incubation time, as the NanoOrange fluorescence was weaker after 16 weeks at 170 °C- and 120 MPa, than after the 4-week incubation at the same conditions. After experimental diagenesis, the fluorescence signal associated with proteins in samples originating from the Fe culture was more intense than in samples originating from the Fe+Si culture. The presence of lipid and polysaccharide components after T–P incubations was evidenced by the fluorescence of associated fluorescent dyes.

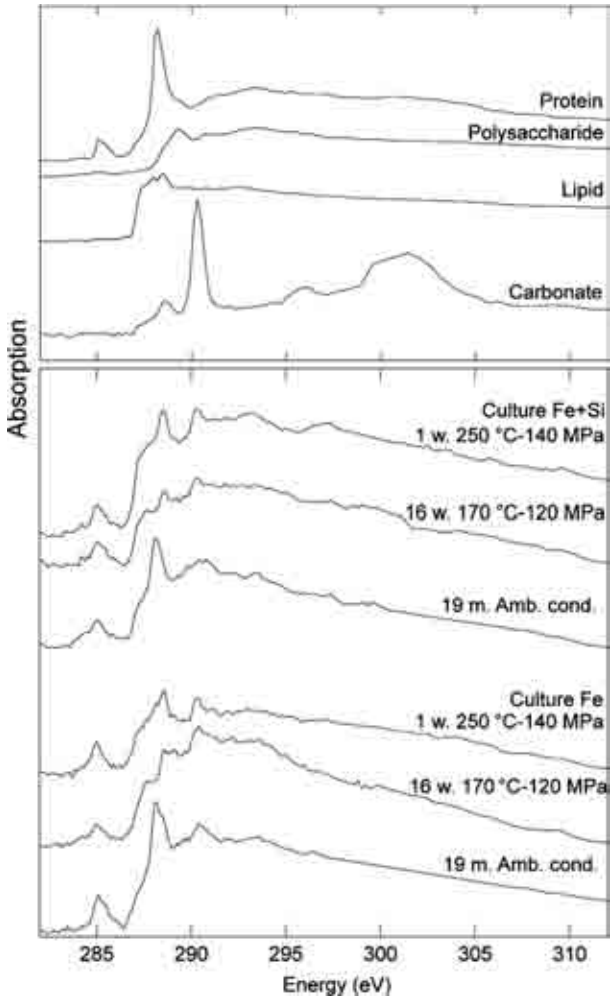


**Fig. 7** Near-edge X-ray absorption fine structure (NEXAFS) spectra at the C K-edge of BoFeN1 cells grown in Fe and Fe+Si before and after incubations under diagenetic conditions. NEXAFS spectra represent averages of whole image sequences. Spectra from 19-month-old cultures (ambient conditions) grown with Fe and Fe+Si did not show significant differences. After incubations under diagenetic conditions, the major absorption peak at 288.2 eV, indicative of $1s \rightarrow \pi^*$ excitations of C=O adjacent to peptide bonds, disappeared from the spectra. Reference spectra for protein, polysaccharide, lipid, and carbonate were from albumin, xanthan, 1,2-dipalmotoyl-sn-glycero-3-phosphocholine, and aragonite, respectively.

**Table 2** Results of the LCF analyses performed on NEXAFS spectra at the C K-edge extracted from image sequences. Normalized standard spectra of protein, polysaccharide, lipid, and carbonate were used. Results are given as calculated percentages

| Experimental conditions | Protein (%) | Polysaccharide (%) | Lipid (%) | Carbonate (%) |
|---|---|---|---|---|
| Culture grown in Fe | | | | |
| 19-month-old culture | 39 | 20 | 28 | 13 |
| 170 °C-120 MPa 16 weeks | – | 37 | 55 | 8 |
| 250 °C-120 MPa 1 week | – | 47 | 45 | 8 |
| Culture grown in Fe+Si | | | | |
| 19-month-old culture | 25 | 13 | 51 | 11 |
| 170 °C-120 MPa 16 weeks | – | 39 | 40 | 9 |
| 250 °C-120 MPa 1 week | – | 36 | 50 | 14 |

NEXAFS, near-edge X-ray absorption fine structure; LCF, linear combination fitting.

## DISCUSSION

### Organo-mineral interactions in microbial cells are stable at ambient conditions

The nitrate-dependent Fe(II)-oxidizing bacterium *Acidovorax* sp. BoFeN1 has been the object of numerous studies to decipher the formation of Fe-mineral crusts around microbial cells and its potential for microbial cell preservation (Kappler *et al.*, 2005; Miot *et al.*, 2009, 2011; Schadler *et al.*, 2009; Klueglein *et al.*, 2014; Schmid *et al.*, 2014). In cultures of BoFeN1 that contained high initial phosphate concentrations, Fe(III) phosphates are the main mineral products of Fe(II) oxidation (Miot *et al.*, 2009). On the other hand, when the initial phosphate concentration is low, similar to our culture conditions, goethite and green rust carbonate are detected after 2 days of incubation, in the close vicinity of cells and loosely around cells, respectively, by TEM-SAED (selected area electron diffraction), NEXAFS at the Fe $L_{3,2}$-edges, X-ray diffraction (XRD), EXAFS at the Fe K-edge and Mössbauer spectroscopy (Pantke *et al.*, 2012). After the completion of Fe(II) oxidation, which occurs after 6–7 days, only goethite is detected, as shown by XRD, EXAFS at the Fe K-edge, NEXAFS at the Fe $L_{3,2}$-edges, and Mössbauer spectroscopy (Hohmann *et al.*, 2010, 2011; Dippon *et al.*, 2012; Pantke *et al.*, 2012; Klueglein *et al.*, 2014). Using XANES spectroscopy, trace levels of ferrihydrite are detected with goethite after 8 days of incubation (Hohmann *et al.*, 2011). After 12–19 months at ambient conditions, goethite was the major mineralogical product in cultures of BoFeN1 (Figs 4 and 5). No apparent Fe(III) reduction occurred over several months at ambient conditions since goethite is known to be very stable at ambient conditions (Cornell & Schwertmann, 2003). Carbonate precipitates were colocalized with Fe, as revealed by STXM (Figs 7 and 8). They were, however, present in trace amounts, as no characteristic peak was observed in the Raman spectra, such as the high-intensity peak at 1087–1094 $cm^{-1}$ corresponding to the $CO_3^{2-}$ symmetric stretching (Gillet *et al.*, 1993). We assumed that some carbonate, used as buffer in the medium, remained adsorbed to the goethite. As Fe(II) is oxidized in a few days, the formation of Fe(II) carbonate can be ruled out. Fe(III) carbonates cannot form because the precipitation of Fe(III) oxyhydr(oxides) prevails. Carbonate is known to direct Fe(III) mineral precipitation toward goethite vs. lepidocrocite or ferrihydrite (Cornell & Schwertmann, 2003).

The main cellular components of BoFeN1 cells were still detectable after 19–21 months, as shown by NEXAFS spectroscopy at the C K-edge and CLSM measurements (Figs 7,

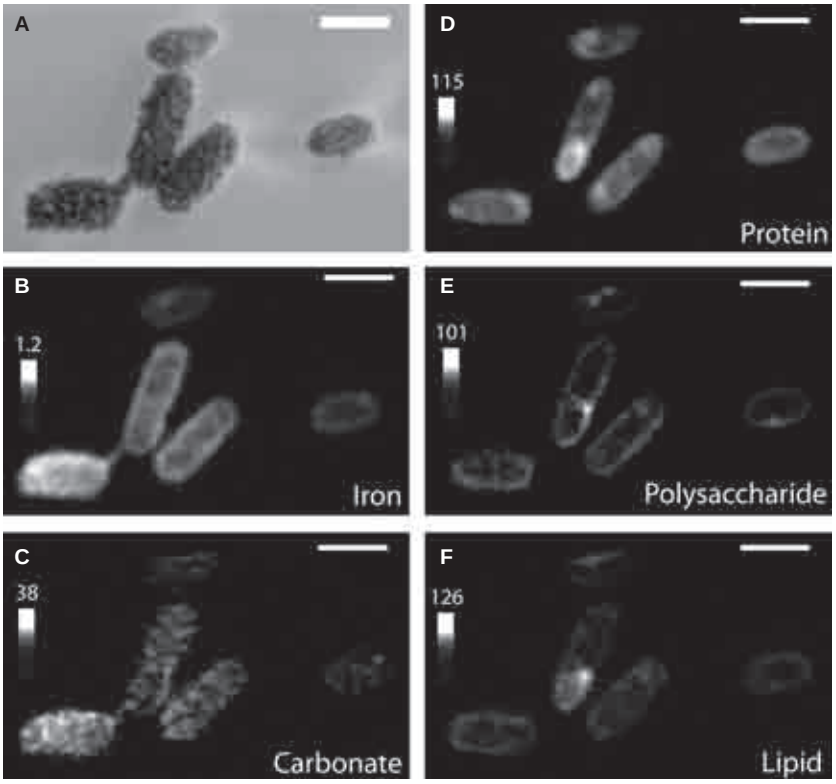


**Fig. 8** BoFeN1 cells from the Fe culture at ambient conditions. SEM image (A), Fe distribution map derived from an image difference (723.8–704 eV) (B), and component maps of protein (albumin standard), polysaccharide (xanthan standard), lipid (1,2-dipalmotoyl-sn-glycero-3-phosphocholine standard), and carbonate (aragonite standard) were derived by LCF of image sequences measured across the C K-edge (280–320 eV). The gray scales indicate OD (Fe map) and thickness in nm (protein, polysaccharide, lipid, and carbonate maps). Scale bars = 1 μm on all images. SEM, scanning electron microscopy; LCF, linear combination fitting; OD, optical density.

8, and 10). Our NEXAFS spectra acquired on 19-month-old cells grown in Fe (Fig. 7) exhibited similar spectral features to those recorded just after Fe(II) oxidation has been completed (Li *et al.*, 2013). During early Fe(II) oxidation, Fe binds to the reactive groups of the peptidoglycan, leading to the encrustation of the periplasm and the preservation of entrapped protein aggregates (Miot *et al.*, 2011). This early mechanism possibly plays a role in the preservation of cellular components, as well as the cell structure (Fig. 1), over 21 months at ambient conditions. Also, in the presence of Fe, BoFeN1 cells produce large amounts of EPS (Klueglein *et al.*, 2014; Fig. 10), additionally providing functional groups for the fixation of $Fe^{3+}$ and further crystallization of Fe minerals (Beveridge, 1989). Therefore, it is plausible that the association of goethite with the cell wall, which occurs mainly through the binding of Fe onto carboxylic and phosphate groups (Beveridge, 1989), plays a role in preserving intact cellular components at ambient conditions.

### High temperature and pressure conditions trigger organo-mineral transformations

In the present study, goethite associated with microbial cells remained stable at ambient conditions, but transformed to hematite and magnetite at conditions above 170 °C-120 MPa and below 250 °C-140 MPa (Fig. 4). In solution, the transformation of pure goethite to hematite occurs directly through hydrothermal dihydroxylation at high temperature (Cornell & Schwertmann, 2003). The goethite-to-hematite conversion temperatures have been estimated to be at 192–250 °C from high-temperature powder XRD measurements (Walter *et al.*, 2001). After 1 week at 250 °C-140 MPa, goethite was still detected in Fe-grown cells, but at low levels (~9%; Figs 4 and 5). The presence of magnetite indicated that some Fe(III) reduction occurred with some oxidation of the organic matter. We have recently demonstrated that organo-mineral twisted stalks treated under similar diagenetic conditions produced the same mineralogical products, that is, hematite and magnetite. However, the transition temperature was at T–P conditions lower than 170 °C-120 MPa, probably because ferrihydrite was the initial Fe(III) mineral (Picard *et al.*, 2015). Similarly, it was shown that ferrihydrite mixed with glucose completely transformed to hematite, magnetite, and siderite after 2 weeks at 170 °C and 120 MPa (Posth *et al.*, 2013).

Organic compounds underwent transformations after 16 weeks at 170 °C-120 MPa (Fig. 7). After experimental diagenesis, the fluorescence signal specific to proteins became very faint and fuzzy (Fig. 10). The peak specific for the amid bond completely disappeared from the NEXAFS spectra at the C K-edge of BoFeN1 cells in Fe cultures after 16 weeks at 170 °C-120 MPa and after 1 week at 250 °C-140 MPa (Fig. 7). In a recent study, similar NEXAFS measurements, performed on high-temperature-treated Fe-encrusted BofeN1 cells, revealed that protein degradation is

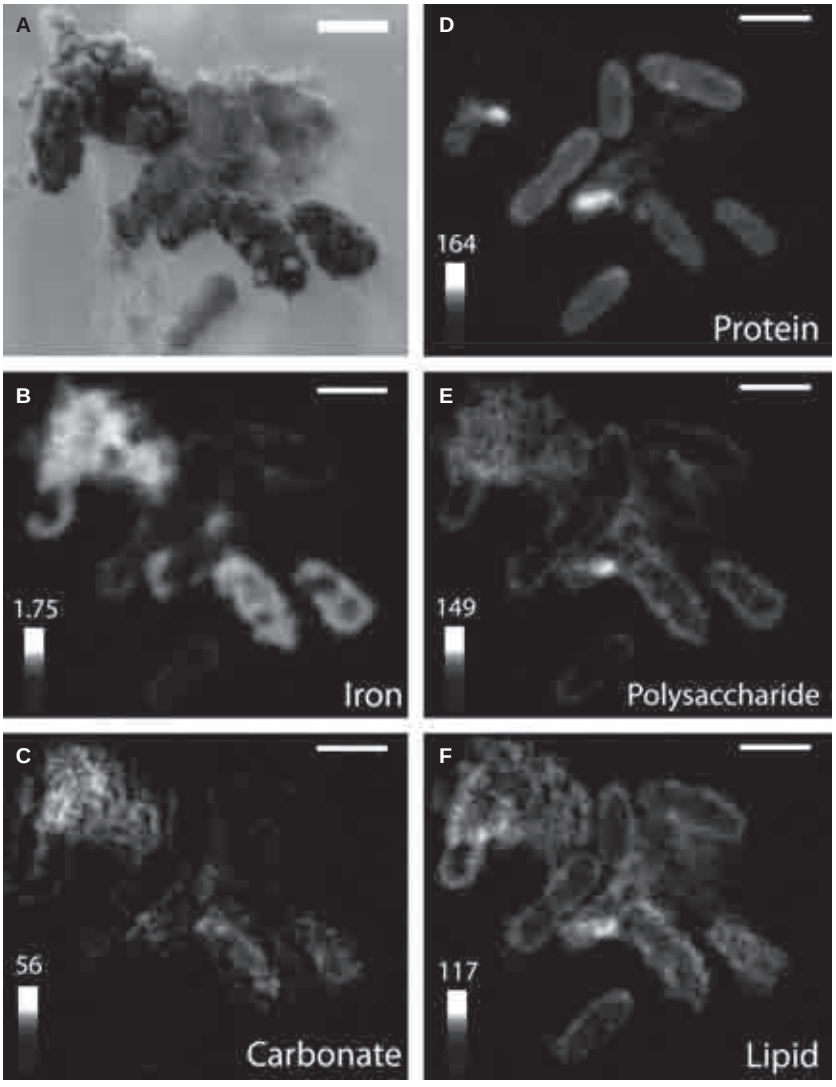


**Fig. 9** BoFeN1 cells from the Fe+Si culture at ambient conditions. SEM image (A), Fe distribution map derived from an image difference (723.8–704 eV) (B), and component maps of protein (albumin standard), polysaccharide (xanthan standard), lipid (1,2-dipalmotoyl-sn-glycero-3-phosphocholine standard), and carbonite (aragonite standard) derived by LCF of image sequences measured across the C K-edge (280–320 eV). The gray scales indicate OD (Fe map) and thickness in nm (protein, polysaccharide, lipid, and carbonate maps). Scale bars = 1 μm on all images. SEM, scanning electron microscopy; LCF, linear combination fitting; OD, optical density.

not completed yet after 100 h at 300 °C and after 20 h at 600 °C, as the peak specific for the amide bond is still present, although significantly less intense (Li *et al.*, 2013). In the case of non-encrusted *E. coli* cells that received the same heating treatment, NEXAFS spectra at the C K-edge are almost completely featureless (Li *et al.*, 2014). This suggests that protein degradation at high temperature can be slowed down but not prevented by the presence of minerals. In our study, the good preservation of lipids and polysaccharides was indicated by the features left in the NEXAFS spectra acquired at the C K-edge (Fig. 7) and by the fluorescent signals obtained by specific fluorescent probes by CLSM (Fig. 10), providing potential molecules for biomarker studies. Recently, we have shown that the main organic components of extracellular organo-mineral twisted stalks produced by microaerophilic Fe(II)-oxidizing bacteria, lipids, and polysaccharides, are preserved under similar diagenetic conditions as used in this study (Picard *et al.*, 2015).

### Role of Si in the preservation of microbial cells in Fe-rich environments and implications for the search of microfossils in rocks

Early Earth environments were much different from modern Earth. Precambrian oceans were anoxic, and before 1.8 Ga were rich in Fe and Si (Holland, 1973; Maliva *et al.*, 2005). To understand the microbial processes that took place at that time, one must be able to decipher the fossil record. Metamorphic conditions of 200–300 °C and <0.7 GPa, as found in the Archean sedimentary record characterized so far, might be already too high to preserve organic biomarkers, such as steranes or hopanes (French *et al.*, 2015). Therefore, in the range of T–P conditions between the former and those of high-grade metamorphism, under which all types of biosignatures are destroyed, the understanding of early life might rely on mineralogical and chemical signals contained in morpho-

logical microfossils. By characterizing the upper pressure and temperature preservation limits of simple systems, such as organic biomarkers, or more complex systems, such as whole cells, one could target the rocks that potentially preserve biosignatures. Despite obvious limitations in terms of incubation time, diagenesis experiments, as performed in this study, allow to estimate the geochemical conditions leading to microfossil preservation and to characterize the kinetics of molecule degradation. As illustrated above, signals exhibited by morphological microfossils after relatively short-term T–P treatments cannot be predicted by long-term incubations at ambient conditions.

The addition of 2 mM of Si to the culture medium of BoFeN1 did not influence the mineralogy of aggregates formed around cells at ambient conditions (Figs 4 and 5). When ferrihydrite forms in cultures of the phototrophic Fe(II)-oxidizing bacterium *Rhodobacter ferrooxidans* SW2 in the presence of 2 mM Si, it is less crystalline than the one formed in the absence of Si and has substitutions of $Fe^{3+}$ by $Si^{4+}$ (Eickhoff *et al.*, 2014). In abiotic goethite synthesis experiments, Si does not substitute for Fe in the crystal structure, but increasing Si concentrations decrease the size of goethite crystals (Mejia Gomez *et al.*, 2011). This seems reflected in the differences in mineral crust morphology observed between Fe and Fe+Si cultures (Fig. 1). Under diagenetic conditions, more goethite was preserved in the presence (~51%) than in the absence of Si (~9%). If the goethite crystals formed in the presence of Si were smaller, they could be packed more tightly in the cell wall or in the EPS, and thus be protected from hydrothermal dehydroxylation to hematite during experimental diagenesis. The amount of magnetite formed during experimental diagenesis in Fe+Si cultures was twice the amount of magnetite formed in the Fe cultures. Therefore, Si did not prevent Fe(II) formation by the coupling of Fe(III) reduction and organic matter oxidation that occur at high T–P conditions. It is possible that the tight association of small goethite particles (formed in the presence of Si) with EPS enhanced the Fe(III) reduction to magnetite. Although in the presence of Si cells became slightly larger after the longest incubation (16 weeks at 170 °C-120 MPa), we infer that the crystal size of the mineral crusts might not have changed significantly with increasing T–P conditions.

The morphology of Fe-encrusted cells was well preserved after incubations at 250 °C-140 MPa for 1 week and at 170 °C-120 MPa for 16 weeks, both in the presence and in the absence of Si (Figs 2, 6, 8–10). A few studies have investigated the fate of microbial cells in thermal aging (temperature) or diagenesis (pressure and temperature) experiments. The shape of *Acidovorax* sp. BoFeN1 cells—grown in Fe for 1 week, then dehydrated—is well preserved after 100 h at 300 °C and 20 h at 600 °C (Li *et al.*, 2013). Similarly, after 1 h at 700 °C, BoFeN1 cells maintain their structural integrity (Miot *et al.*, 2014). *Escherichia coli* cells encrusted in phosphate minerals are well preserved after 100 h at 300 °C and 20 h at 600 °C (Li *et al.*, 2014), although not as well as Fe-encrusted BoFeN1 cells after the same heating conditions (Li *et al.*, 2013). While mineral-encrusted cells seem to sustain high-temperature conditions, cells of *Bacillus subtilis* bound to the cation $Fe^{3+}$ are destroyed after moderate heating at 100 °C (Beveridge *et al.*, 1983). This suggests that a successful preservation of cell structures could be achieved only if minerals have formed before the onset of experimental diagenetic conditions. In BoFeN1 cells, Fe binding on the outer side of the plasma membrane leads to nucleation and growth of Fe minerals in the periplasm within 1 day, setting up favorable conditions for preservation under high T–P conditions (Miot *et al.*, 2011). Although cells grown in Fe and Fe+Si cultures presented crust morphologies distinctive from one another (Fig. 1), and the difference in mineral crust morphology was still observed after experimental diagenesis, these morphologies were found in the same culture of strain BoFeN1 grown in the presence of Fe only in a low-phosphate medium at ambient conditions (Schmid *et al.*, 2014). Therefore, in our experimental conditions, the morphology of mineral crusts around cells does not have a significant value to inform on the geochemistry of fluids present during mineral precipitation.

Near-edge X-ray absorption fine structure spectroscopy and CLSM did not point at differences in the organic matter composition in the presence of Si at ambient conditions in comparison with cells grown without Si. Additionally, Si did not prevent the degradation of organic matter during experimental diagenesis (Figs 7–10). After 1 year in Si, *Methanocaldococcus jannaschii* cells are not preserved but amino acids and fatty acids can still be detected in the cultures (Orange *et al.*, 2012). Actually, this strain has been shown to preserve its cell integrity in Si only after binding $Fe^{3+}$ (Orange *et al.*, 2011). Similarly, $Fe^{3+}$ significantly improved the preservation of Bacillus subtilis in Si at ambient conditions, by inhibiting autocatalytic enzymes (Ferris *et al.*, 1988). This suggests that Fe helps preserving better cell morphology and cellular content than Si alone. In earlier studies, cyanobacterial cells and sheaths that had Si polymerized on their surfaces showed little degradation after 31 weeks at 100 °C and 300 MPa, but were highly degraded after 3–4 weeks at 165 °C-300 MPa (Oehler & Schopf, 1971; Oehler, 1976). This also suggests that Fe could help preserving cellular components and structure at higher T–P conditions. This hypothesis could be tested by subjecting samples from modern Fe- and Si-rich environments to experimental diagenesis. For example, in hot springs, the composition of mineral crusts depends on the composition of the fluids where mats develop; in fluids richer in Si, amorphous Si-rich spheroidal grains develop in capsules and on cell walls and can eventually grow into

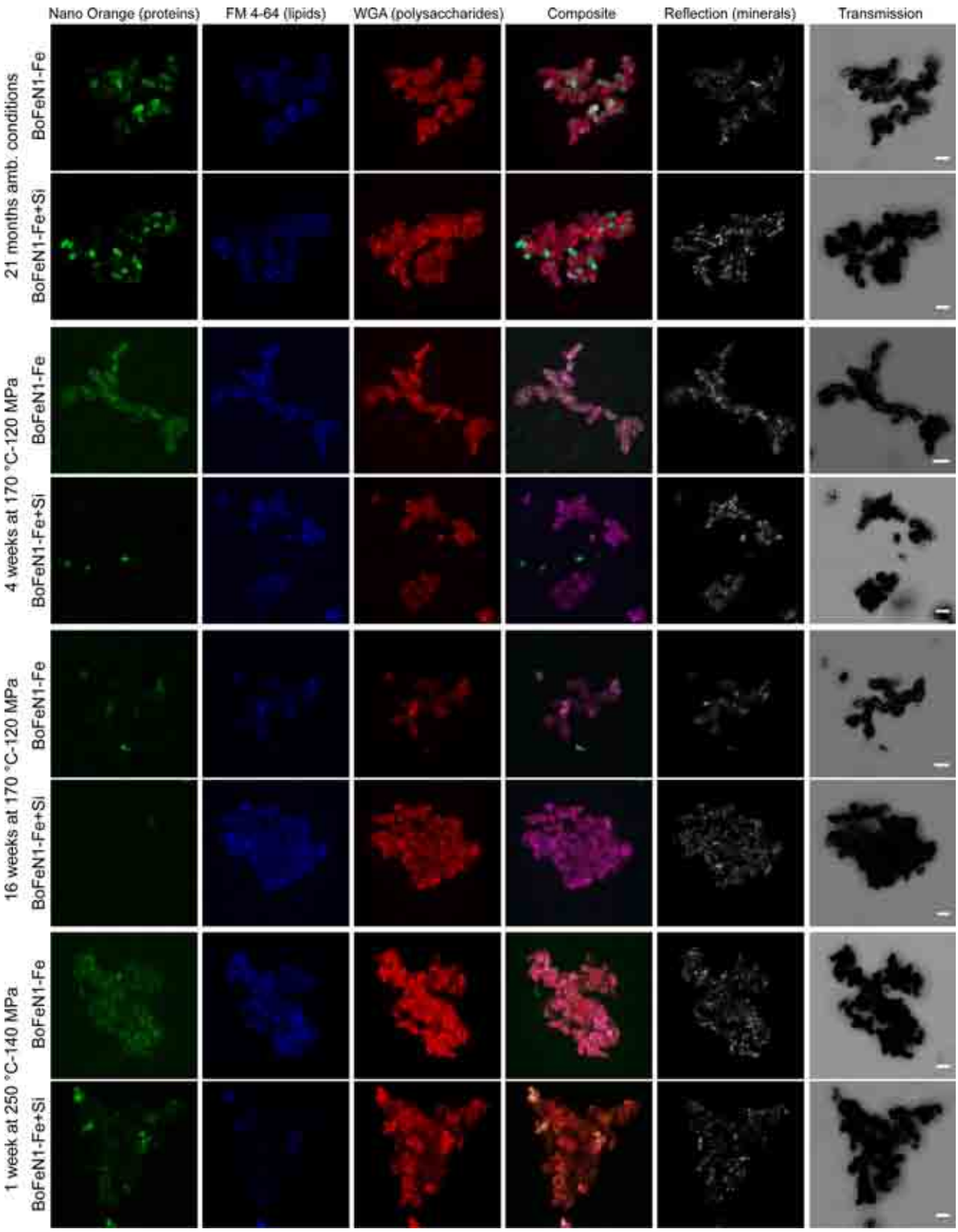

**Fig. 10** Confocal laser scanning microscopy images of *Acidovorax* sp. BoFeN1 incubated with Fe (row 1) and Fe+Si (row 2) for 21 months, and after incubations of those cultures for 4 weeks (rows 3 and 4) and 16 weeks (rows 5 and 6) at 170 °C-120 MPa, and for 1 week at 250 °C-140 MPa (rows 7 and 8). Proteins were stained with NanoOrange (green), lipids with FM4-64 (blue), and polysaccharides with WGA-Alexa Fluor 633 (red). The composite image is a RGB overlay of the first three images on the left. The gray panel shows the reflection of minerals, while the last panel on the right shows the transmission through the cell aggregates. Scale bars = 1 μm. Each scale bar is applicable to the whole row of images.

thick layers, while in Fe-rich that contain low concentrations of Si, mineral crusts of fine-grained ferrihydrite and acicular goethite precipitates develop at the cell surface (Konhauser & Ferris, 1996). When Si and Fe are present at the same time in the fluids, the main mineral precipitates forming on micro-organisms are Fe silicates (Ferris *et al.*, 1986; Konhauser, 1997; Fortin *et al.*, 1998). Comparing preservation of these different patterns after experimental diagenesis could help understand selective preservation during microbial fossilization.

Fe encrustation is not a feature common to all Fe(II) oxidizers, as phototrophic Fe(II)-oxidizing bacteria remain mostly free of their Fe(III) mineral byproducts (Schadler *et al.*, 2009). But as Fe(II) oxidation in nitrate-rich environments seems to be mediated by an abiotic reaction with nitrite produced by denitrification (Melton *et al.*, 2014), many nitrate reducers, not only BoFeN1, can become encrusted in the presence of Fe(II) (Klueglein *et al.*, 2014; Park *et al.*, 2014), suggesting that Fe encrustation is a potential important way of preserving cells living in anoxic Fe-rich environments. Therefore, preservation of morphological microfossils embedded in Fe minerals could be expected in Fe-rich rocks. For example, coccoid microfossils, reaching up to 10 μm in size, and associated with graphite, goethite, and hematite, were described in the 1.9-Ga Gunflint formation (Tazaki *et al.*, 1992). The absence of magnetite in the latter example is striking as graphite has replaced cells, suggesting a complete oxidation of the organic matter. Our experimental results could support the 'biological model' that explains the presence of hematite-coated microfossils through diagenesis of Fe-encrusted minerals, rather than the 'taphonomic model' that proposes the late mineralization of carbonaceous microfossils (Shapiro & Konhauser, 2015). However, it is important to consider the depositional environment in every situation. In that regard, new analytical approaches allowing 3D nanoscale reconstructions, such as focused ion beam (FIB)-TEM and 3-D FIB-SEM associated with nanoscale elemental mapping, have provided unprecedented insights into the microbial fossil record (Brasier *et al.*, 2015). It is thus suggested that a combination of nanoscale methods, if possible including 3-D reconstructions, be applied to future biomineralization studies, as recently applied for BoFeN1 cells (Miot *et al.*, 2011; Schmid *et al.*, 2014), and to the characterization of experimentally made microfossils. More generally, experimental diagenesis experiments could provide constraints on the conditions that lead to the preservation of cells in minerals, as well as the redox state of C and minerals.

## ACKNOWLEDGMENTS

STXM measurements were done at beamline 5.3.2.2 of the Advanced Light Source, Berkeley, CA. The Advanced Light Source is supported by the Director, Office of Science, Office of Basic Energy Sciences, of the U.S. Department of Energy under Contract No. DE-AC02-05CH11231. We thank David Kilcoyne for excellent support at the beamline. Reference spectra at the O1s edge were measured at the spectromicroscopy beamline 10ID-1 of the Canadian Light Source, which is supported by the Canadian Foundation for Innovation, Natural Sciences and Engineering Research Council of Canada, the University of Saskatchewan, the Government of Saskatchewan, Western Economic Diversification Canada, the National Research Council Canada, and the Canadian Institute of Health Research. We thank the beamline staff for assistance during measurements. We thank Dr. Hartmut Schulz for assistance at the SEM, Prof. Dr. Martin Wahl for providing access to the Raman spectrometer at the Institute of Pharmaceutical Sciences (Pharmaceutical Technology, University of Tübingen), and to Ellen Struve for support in the laboratory. We are thankful to Elizabeth Swanner for fruitful discussions. This work was supported by DFG grants KA1736/18-1 and OB 362/1-1.

## REFERENCES

Barghoorn ES, Tyler SA (1965) Microorganisms from Gunflint chert – these structurally preserved Precambrian fossils from Ontario are most ancient organisms known. *Science* **147**, 563–577.

Beveridge TJ (1989) Role of cellular design in metal accumulation and mineralization. *Annual Review of Microbiology* **43**, 147–171.

Beveridge TJ, Meloche JD, Fyfe WS, Murray RG (1983) Diagenesis of metals chemically complexed to bacteria: laboratory formation of metal phosphates, sulfides, and organic condensates in artificial sediments. *Applied and Environmental Microbiology* **45**, 1094–1108.

Brasier MD, Green OR, Jephcoat AP, Kleppe AK, Van Kranendonk MJ, Lindsay JF, Steele A, Grassineau NV (2002) Questioning the evidence for Earth's oldest fossils. *Nature* **416**, 76–81.

Brasier MD, Antcliffe J, Saunders M, Wacey D (2015) Changing the picture of Earth's earliest fossils (3.5–1.9 Ga) with new approaches and new discoveries. *Proceedings of the National*

*Academy of Sciences of the United States of America* **112**, 4859–4864.
Cornell RM, Schwertmann U (2003) *The Iron Oxides: Structure, Properties, Reactions, Occurrences and Uses*. Wiley VCH Verlag, Darmstadt.
Das S, Hendry MJ (2011) Application of Raman spectroscopy to identify iron minerals commonly found in mine wastes. *Chemical Geology* **290**, 101–108.
Dippon U, Pantke C, Porsch K, Larese-Casanova P, Kappler A (2012) Potential function of added minerals as nucleation sites and effect of humic substances on mineral formation by the nitrate-reducing Fe(II)-oxidizer *Acidovorax* sp. BoFeN1. *Environmental Science & Technology* **46**, 6556–6565.
Dynes JJ, Lawrence JR, Korber DR, Swerhone GDW, Leppard GG, Hitchcock AP (2006) Quantitative mapping of chlorhexidine in natural river biofilms. *Science of the Total Environment* **369**, 369–383.
Ehrenreich A, Widdel F (1994) Anaerobic oxidation of ferrous iron by purple bacteria, a new type of phototrophic metabolism. *Applied and Environmental Microbiology* **60**, 4517–4526.
Eickhoff M, Obst M, Schröder C, Hitchcock AP, Tyliszczak T, Martinez RE, Robbins LJ, Konhauser KO, Kappler A (2014) Nickel partitioning in biogenic and abiogenic ferrihydrite: the influence of silica and implications for ancient environments. *Geochimica et Cosmochimica Acta* **140**, 65–79.
Fein JB, Scott S, Rivera N (2002) The effect of Fe on Si adsorption by *Bacillus subtilis* cell walls: insights into non-metabolic precipitation of silicate minerals. *Chemical Geology* **182**, 265–273.
Ferris FG, Beveridge TJ, Fyfe WS (1986) Iron-silica crystallite nucleation by bacteria in a geothermal sediment. *Nature* **320**, 609–611.
Ferris FG, Fyfe WS, Beveridge TJ (1987) Bacteria as nucleation sites for authigenic minerals in a metal-contaminated lake sediment. *Chemical Geology* **63**, 225–232.
Ferris FG, Fyfe WS, Beveridge TJ (1988) Metallic ion binding by *Bacillus subtilis* – implications for the fossilization of microorganisms. *Geology* **16**, 149–152.
Fortin D, Ferris FG, Scott SD (1998) Formation of Fe-silicates and Fe-oxides on bacterial surfaces in samples collected near hydrothermal vents on the Southern Explorer Ridge in the northeast Pacific Ocean. *American Mineralogist* **83**, 1399–1408.
Francis S, Margulis L, Barghoorn ES (1978) On the experimental silicification of microorganisms. II. On the time of appearance of eukaryotic organisms in the fossil record. *Precambrian Research* **6**, 65–100.
French KL, Hallmann C, Hope JM, Schoon PL, Zumberge JA, Hoshino Y, Peters CA, George SC, Love GD, Brocks JJ, Buick R, Summons RE (2015) Reappraisal of hydrocarbon biomarkers in Archean rocks. *Proceedings of the National Academy of Sciences of the United States of America* **112**, 5915–5920.
Gillet P, Biellmann C, Reynard B, Mcmillan P (1993) Raman spectroscopic studies of carbonates. 1. High-pressure and high-temperature behavior of calcite, magnesite, dolomite and aragonite. *Physics and Chemistry of Minerals* **20**, 1–18.
Hitchcock AP (2015) aXis2000 is an IDL-based analytical package, available at http://unicorn.macmaster.ca/axis2000.html.
Hohmann C, Winkler E, Morin G, Kappler A (2010) Anaerobic Fe(II)-oxidizing bacteria show as resistance and immobilize as during Fe(III) mineral precipitation. *Environmental Science & Technology* **44**, 94–101.
Hohmann C, Morin G, Ona-Nguema G, Guigner JM, Brown GE, Kappler A (2011) Molecular-level modes of As binding to Fe (III) (oxyhydr)oxides precipitated by the anaerobic nitrate-reducing Fe(II)-oxidizing *Acidovorax* sp. strain BoFeN1. *Geochimica et Cosmochimica Acta* **75**, 4699–4712.
Holland HD (1973) The oceans: a possible source of iron in iron formations. *Economic Geology* **68**, 1169–1172.
Kappler A, Schink B, Newman DK (2005) Fe(III) mineral formation and cell encrustation by the nitrate-dependent Fe(II)-oxidizer strain BoFeN1. *Geobiology* **3**, 235–245.
Kaznatcheev KV, Karunakaran C, Lanke UD, Urquhart SG, Obst M, Hitchcock AP (2007) Soft X-ray spectromicroscopy beamline at the CLS: commissioning results. *Nuclear Instruments & Methods in Physics Research Section A: Accelerators Spectrometers Detectors and Associated Equipment* **582**, 96–99.
Kilcoyne ALD, Tyliszczak T, Steele WF, Fakra S, Hitchcock P, Franck K, Anderson E, Harteneck B, Rightor EG, Mitchell GE, Hitchcock AP, Yang L, Warwick T, Ade H (2003) Interferometer-controlled scanning transmission X-ray microscopes at the Advanced Light Source. *Journal of Synchrotron Radiation* **10**, 125–136.
Klueglein N, Zeitvogel F, Stierhof YD, Floetenmeyer M, Konhauser KO, Kappler A, Obst M (2014) Potential role of nitrite for abiotic Fe(II) oxidation and cell encrustation during nitrate reduction by denitrifying bacteria. *Applied and Environmental Microbiology* **80**, 1051–1061.
Konhauser KO (1997) Bacterial iron biomineralisation in nature. *FEMS Microbiology Reviews* **20**, 315–326.
Konhauser KO (1998) Diversity of bacterial iron mineralization. *Earth-Science Reviews* **43**, 91–121.
Konhauser KO, Ferris FG (1996) Diversity of iron and silica precipitation by microbial mats hydrothermal waters, Iceland: implications for Precambrian iron formations. *Geology* **24**, 323–326.
Konhauser KO, Jones B (2011) Microbial silicification – bacteria (or passive). In *Encyclopedia of Geobiology*. (eds Reitner J, Thiel V). Springer, Netherlands, pp. 608–613.
Konhauser KO, Fisher QJ, Fyfe WS, Longstaffe FJ, Powell MA (1998) Authigenic mineralization and detrital clay binding by freshwater biofilms: the Brahmani River, India. *Geomicrobiology Journal* **15**, 209–222.
Konhauser KO, Jones B, Phoenix V, Ferris G, Renaut R (2004) The microbial role in hot spring silicification. *Ambio* **33**, 552–558.
Lalonde SV, Konhauser KO, Reysenbach AL, Ferris FG (2005) The experimental silicification of Aquificales and their role in hot spring sinter formation. *Geobiology* **3**, 41–52.
Lawrence JR, Swerhone GDW, Leppard GG, Araki T, Zhang X, West MM, Hitchcock AP (2003) Scanning transmission X-ray, laser scanning, and transmission electron microscopy mapping of the exopolymeric matrix of microbial biofilms. *Applied and Environmental Microbiology* **69**, 5543–5554.
Lehmann J, Solomon D, Brandes J, Fleckenstein H, Jacobson C, Thieme J (2009) Synchrotron-based near-edge X-ray spectroscopy of NOM in soils and sediments. In *Biophysico-Chemical Processes Involving Natural Nonliving Organic Matter in Environmental Systems*. (eds Senesi N, Xing B, Huang PM). Wiley, Hoboken, New Jersey, pp. 723–775.
Li J, Benzerara K, Bernard S, Beyssac O (2013) The link between biomineralization and fossilization of bacteria: insights from field and experimental studies. *Chemical Geology* **359**, 49–69.
Li J, Bernard S, Benzerara K, Beyssac O, Allard T, Cosmidis J, Moussou J (2014) Impact of biomineralization on the preservation of microorganisms during fossilization: an

experimental perspective. *Earth and Planetary Science Letters* **400**, 113–122.
Maliva RG, Knoll AH, Simonson BM (2005) Secular change in the Precambrian silica cycle: insights from chert petrology. *Geological Society of America Bulletin* **117**, 835–845.
Mejia Gomez JA, De Resende VG, Antonissen J, De Grave E (2011) Characterization of the effects of silicon on the formation of goethite. *Corrosion Science* **53**, 1756–1761.
Melton ED, Swanner ED, Behrens S, Schmidt C, Kappler A (2014) The interplay of microbially mediated and abiotic reactions in the biogeochemical Fe cycle. *Nature Reviews Microbiology* **12**, 797–808.
Miot J, Benzerara K, Morin G, Kappler A, Bernard S, Obst M, Ferard C, Skouri-Panet F, Guigner JM, Posth N, Galvez M, Brown GE, Guyot F (2009) Iron biomineralization by anaerobic neutrophilic iron-oxidizing bacteria. *Geochimica et Cosmochimica Acta* **73**, 696–711.
Miot J, Maclellan K, Benzerara K, Boisset N (2011) Preservation of protein globules and peptidoglycan in the mineralized cell wall of nitrate-reducing, iron(II)-oxidizing bacteria: a cryo-electron microscopy study. *Geobiology* **9**, 459–470.
Miot J, Recham N, Larcher D, Guyot F, Brest J, Tarascon JM (2014) Biomineralized alpha-$Fe_2O_3$: texture and electrochemical reaction with Li. *Energy & Environmental Science* **7**, 451–460.
Obst M, Dynes JJ, Lawrence JR, Swerhone GDW, Benzerara K, Karunakaran C, Kaznatcheev K, Tyliszczak T, Hitchcock AP (2009) Precipitation of amorphous $CaCO_3$ (aragonite-like) by cyanobacteria: a STXM study of the influence of EPS on the nucleation process. *Geochimica et Cosmochimica Acta* **73**, 4180–4198.
Oehler JH (1976) Experimental studies in Precambrian paleontology – structural and chemical changes in blue-green algae during simulated fossilization in synthetic chert. *Geological Society of America Bulletin* **87**, 117–129.
Oehler JH, Schopf JW (1971) Artificial microfossils: experimental studies of permineralization of blue-green algae in silica. *Science* **174**, 1229–1231.
Orange F, Westall F, Disnar JR, Prieur D, Bienvenu N, Leromancer M, Defarge C (2009) Experimental silicification of the extremophilic archaea *Pyrococcus abyssi* and *Methanocaldococcus jannaschii*: applications in the search for evidence of life in early Earth and extraterrestrial rocks. *Geobiology* **7**, 403–418.
Orange F, Disnar JR, Westall F, Prieur D, Baillif P (2011) Metal cation binding by the hyperthermophilic microorganism, archaea *Methanocaldococcus jannaschii,* and its effects on silicification. *Palaeontology* **54**, 953–964.
Orange F, Disnar JR, Gautret P, Westall F, Bienvenu N, Lottier N, Prieur D (2012) Preservation and evolution of organic matter during experimental fossilisation of the hyperthermophilic archaea *Methanocaldococcus jannaschii. Origins of Life and Evolution of the Biosphere* **42**, 587–609.
Orange F, Lalonde SV, Konhauser KO (2013a) Experimental simulation of evaporation-driven silica sinter formation and microbial silicification in hot spring systems. *Astrobiology* **13**, 163–176.
Orange F, Lalonde SV, Konhauser KO (2013b) The formation and preservation of *Synechococcus elongatus* cell molds in simulated silica sinter: implications for the identification of microfossils. *Geomicrobiology Journal* **30**, 327–336.
Orange F, Dupont S, Le Goff O, Bienvenu N, Disnar JR, Westall F, Le Romancer M (2014) Experimental fossilization of the thermophilic Gram-positive bacterium *Geobacillus* SP7A: a long duration preservation study. *Geomicrobiology Journal* **31**, 578–589.
Pantke C, Obst M, Benzerara K, Morin G, Ona-Nguema G, Dippon U, Kappler A (2012) Green rust formation during Fe (II) oxidation by the nitrate-reducing *Acidovorax* sp. strain BoFeN1. *Environmental Science & Technology* **46**, 1439–1446.
Park S, Kim DH, Lee JH, Hur HG (2014) *Sphaerotilus natans* encrusted with nanoball-shaped Fe(III) oxide minerals formed by nitrate-reducing mixotrophic Fe(II) oxidation. *FEMS Microbiology Ecology* **90**, 68–77.
Phoenix VR, Konhauser KO, Ferris FG (2003) Experimental study of iron and silica immobilization by bacteria in mixed Fe-Si systems: implications for microbial silicification in hot springs. *Canadian Journal of Earth Sciences* **40**, 1669–1678.
Picard A, Kappler A, Schmid G, Quaroni L, Obst M (2015) Experimental diagenesis of organo-mineral structures formed by microaerophilic Fe(II)-oxidizing bacteria. *Nature Communications* **6**, 6277.
Posth NR, Kohler I, Swanner ED, Schroder C, Wellmann E, Binder B, Konhauser KO, Neumann U, Berthold C, Nowak M, Kappler A (2013) Simulating Precambrian banded iron formation diagenesis. *Chemical Geology* **362**, 66–73.
Schadler S, Burkhardt C, Hegler F, Straub KL, Miot J, Benzerara K, Kappler A (2009) Formation of cell-iron-mineral aggregates by phototrophic and nitrate-reducing anaerobic Fe(II)-oxidizing bacteria. *Geomicrobiology Journal* **26**, 93–103.
Schmid G, Zeitvogel F, Hao L, Ingino P, Floetenmeyer M, Stierhof YD, Schroeppel B, Burkhardt CJ, Kappler A, Obst M (2014) 3-D analysis of bacterial cell-(iron)mineral aggregates formed during Fe(II) oxidation by the nitrate-reducing *Acidovorax* sp. strain BoFeN1 using complementary microscopy tomography approaches. *Geobiology* **12**, 340–361.
Schopf JW (1993) Microfossils of the early Archean Apex chert: new evidence of the antiquity of life. *Science* **260**, 640–646.
Schopf JW, Kudryavtsev AB, Agresti DG, Wdowiak TJ, Czaja AD (2002) Laser-Raman imagery of Earth's earliest fossils. *Nature* **416**, 73–76.
Shapiro RS, Konhauser KO (2015) Hematite-coated microfossils: primary ecological fingerprint or taphonomic oddity of the Paleoproterozoic? *Geobiology* **13**, 209–224.
Siever R (1992) The silica cycle in the Precambrian. *Geochimica et Cosmochimica Acta* **56**, 3265–3272.
Tazaki K, Ferris FG, Wiese RG, Fyfe WS (1992) Iron and graphite associated with fossil bacteria in chert. *Chemical Geology* **95**, 313–325.
Toporski JKW, Steele A, Westall F, Thomas-Keprta KL, Mckay DS (2002) Winner of the 2001 Gerald A. Soffen Memorial Award – the simulated silicification of bacteria – new clues to the modes and timing of bacterial preservation and implications for the search for extraterrestrial microfossils. *Astrobiology* **2**, 1–26.
Urrutia MM, Beveridge TJ (1993) Mechanism of silicate binding to the bacterial cell wall in *Bacillus subtilis. Journal of Bacteriology* **175**, 1936–1945.
Urrutia MM, Beveridge TJ (1994) Formation of fine-grained metal and silicate precipitates on a bacterial surface (*Bacillus subtilis*). *Chemical Geology* **116**, 261–280.
Walter D, Buxbaum G, Laqua W (2001) The mechanism of the thermal transformation from goethite to hematite. *Journal of Thermal Analysis and Calorimetry* **63**, 733–748.
Westall F (2008) Morphological biosignatures in early terrestrial and extraterrestrial materials. *Space Science Reviews* **135**, 95–114.
Westall F, Boni L, Guerzoni E (1995) The experimental silicification of microorganisms. *Palaeontology* **38**, 495–528.

## SUPPORTING INFORMATION

Additional Supporting Information may be found in the online version of this article:

**Fig. S1** Cultures of *Acidovorax* sp. BoFeN1 grown in anoxic freshwater medium with acetate, nitrate and Fe(II) in the absence (left) or presence (right) of Si. The picture was taken directly after shaking the bottles by hand. While Fe minerals attach to the glass bottle when Si is absent, Fe minerals stay loose in the presence of Si.

**Fig. S2** BoFeN1 cells grown in Fe and Fe+Si after incubation for 4 months at 170 °C-120 MPa. From left to right: SEM image, Fe distribution map derived from an image difference (723.8–704 eV) and component maps of carbonate (aragonite standard), polysaccharide (xanthan standard) and lipid (1,2-dipalmotoyl-sn-glycero-3-phosphocholine standard), derived by LCF of image sequences measured across the C K-edge (280–320 eV). The grey scales indicate OD (Fe map) and thickness in nm (carbonate, polysaccharide and lipid maps). Scale bars = 1 μm on all images. SEM, scanning electron microscopy; OD, optical density; LCF, linear combination fitting.

**Fig. S3** BoFeN1 cells grown in Fe and Fe+Si after incubation for 1 week at 250 °C-140 MPa. From left to right: SEM image, Fe distribution map derived from an image difference (723.8–704 eV) and component maps of carbonate (aragonite standard), polysaccharide (xanthan standard) and lipid (1,2-dipalmotoyl-sn-glycero-3-phosphocholine standard), derived by LCF of image sequences measured across the C K-edge (280–320 eV). The grey scales indicate OD (Fe map) and thickness in nm (carbonate, polysaccharide and lipid maps). Scale bars = 1 μm on all images. SEM, scanning electron microscopy; OD, optical density; LCF, linear combination fitting.

**Table S1** Analysis of the cell length in BoFeN1 cultures grown in Fe and Fe+Si as a function of T–P conditions. The cell length (μm) was measured on SEM images. A one-way ANOVA was performed with the Kaleidagraph application ($F = 3.4030223$, $P = 0.0004$). A Dunnett post-hoc test was performed for all data against the data of BoFeN1 cells grown in Fe (ambient conditions). *P* from Dunnett's multiple comparison tests are given in the table. BoFeN1 cells grown in Fe+Si and incubated at 170 °C-120 MPa for 16 weeks are significantly longer than cells before T–P treatment.